Late Holocene glacier and climate fluctuations in the Mackenzie and Selwyn Mountain Ranges, Northwest Canada

Adam C. Hawkins[1], Brian Menounos[1,2], Brent M. Goehring[3], Gerald Osborn[4], Ben M. Pelto[5], Christopher M. Darvill[6], Joerg M. Schaefer[7]

5   [1]Department of Geography, Earth, and Environmental Science, University of Northern British Columbia, Prince George, V2M 5Z9, Canada
[2]Hakai Institute, Campbell River, V9W 2C7, Canada
[3]Los Alamos National Laboratory, Los Alamos, 87545, USA
[4]Department of Geoscience, University of Calgary, Calgary, T2N 1N4, Canada
10 [5]Department of Geography, University of British Columbia, Vancouver, V6T 1Z4, Canada
[6]Department of Geography, University of Manchester, Manchester M13 9PL, England
[7]Department of Earth and Environmental Sciences, Lamont-Doherty Earth Observatory, Columbia University, Palisades, 10964, USA

Correspondence to: Adam C. Hawkins (ahawkins@unbc.ca)

Abstract. Over the last century, northwestern Canada experienced some of the highest rates of tropospheric warming globally, which caused glaciers in the region to rapidly retreat. Our study seeks to extend the record of glacier fluctuations and assess climate drivers prior to the instrumental record in the Mackenzie and Selwyn Mountains of northwestern Canada. We collected 27 [10]Be surface exposure ages across nine cirque and valley glacier moraines to constrain the timing of their emplacement. Cirque and valley glaciers in this region reached their greatest Holocene extents in the latter half of the Little Ice Age (1600-1850 CE). Four erratics, 10-250 m distal from late Holocene moraines, yielded [10]Be exposure ages of 10.9-11.6 ka, demonstrating that by ca. 11 ka, alpine glaciers were no more extensive than during the last several hundred years. Estimated temperature change obtained through reconstruction of equilibrium line altitudes show that since ca. 1850 CE, mean annual temperatures rose 0.2-2.3 °C. We use our glacier chronology and the Open Global Glacier Model (OGGM) to estimate that since 850 CE, glaciers in this region reached a maximum total volume of 34-38 km^3 between 1765-1855 CE and have lost nearly half their ice volume by 2019 CE. OGGM was unable to produce modeled glacier lengths that match the timing or magnitude of the maximum glacier extent indicated by the [10]Be chronology. However, when applied to the entire Mackenzie and Selwyn Mountain region, past-millennium OGGM simulations using the Max Planck Institute Earth System Model (MPI-ESM) and the Community Climate System Model 4 (CCSM4) yield late Holocene glacier volume change temporally consistent with our moraine and remote sensing record, while the Meteorological Research Institute Earth System Model 2 (MRI-ESM2) and the Model for Interdisciplinary Research on Climate (MIROC) fail to produce modeled glacier change consistent with our glacier chronology. Finally, OGGM forced by future climate projections under varying greenhouse gas emissions scenarios predict 85 to over 97% glacier volume loss by the end of the 21st century. The loss of glaciers from this region will have profound impacts to local ecosystems and communities that rely on meltwaters from glacierized catchments.

1 Introduction

Between 1990-2020 CE, northwestern Canada warmed by 1.1 °C above the 1961-1990 CE average (Muñoz-Sabater, 2019, 2021), which contributed to the loss of an estimated 0.429 ± 0.232 km^3 of ice in the Mackenzie and Selwyn Mountains of eastern Yukon and Northwest Territories between 2000 and 2020 CE (Fig. 1; Hugonnet et al., 2021). Glaciers in this region are clearly responding to recent climate warming, but proxy evidence of past climate change is scarce (Tomkins et al., 2008; Dyke, 1990). Reconstructions of when and how glaciers responded to past climate change provide one method for estimating paleoclimatic conditions, while also placing the rate of modern glacier change into a geologic context.
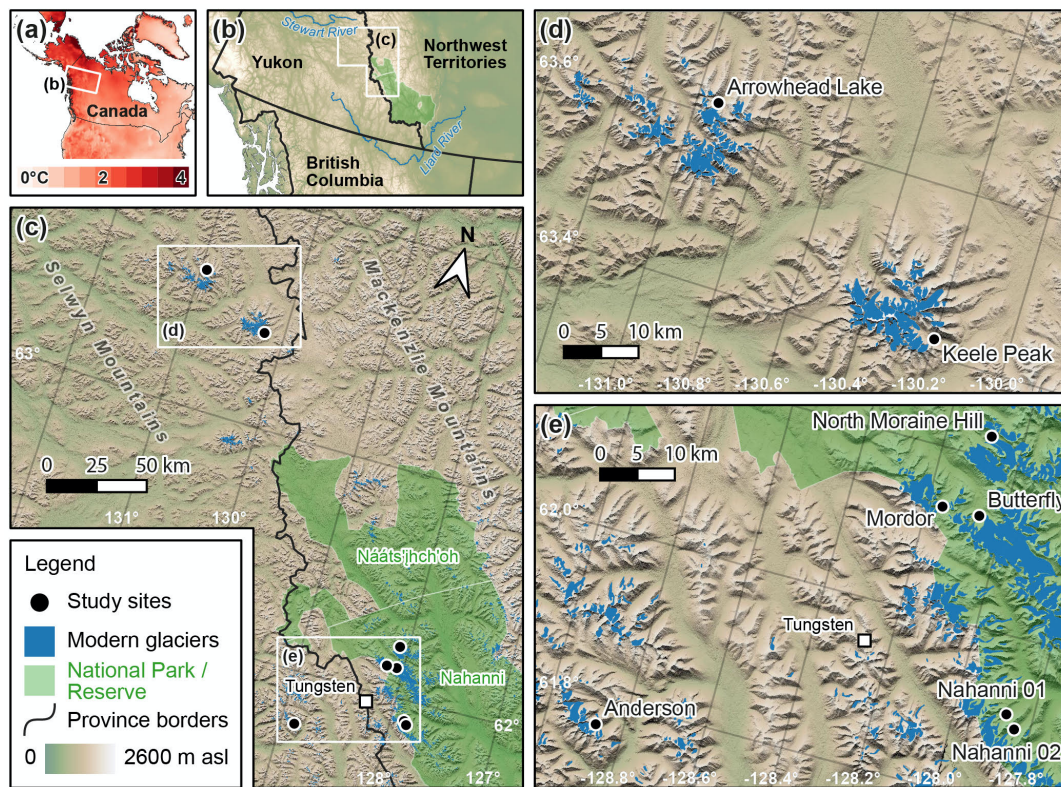
Figure 1: Study area map of ^{10}Be sampling locations. Panel (a) is the temperature trend from ERA5land between 1950 and 2021 CE.

Few glacier change studies exist for the Mackenzie and Selwyn Mountains as compared to other mountainous regions in SW Yukon, British Columbia, and Alaska. Previous Quaternary research in this region focused on Pleistocene glacial deposits and Holocene rock glaciers (i.e. Duk-Rodkin et al., 1996; Fritz et al., 2012; Menounos et al., 2017; Dyke, 1990). The remote location and related logistical challenges of conducting fieldwork in this area are likely reasons this region is underrepresented in Holocene climate reconstructions (e.g. Marcott et al., 2013).

Research in northern and interior Alaska indicates that glaciers reached their maximum Holocene extents around 3.0-2.0 ka (Badding et al., 2013) while nearly all glaciers in southern Alaska and western Canada reached their greatest Holocene positions at the culmination of the Little Ice Age (LIA, ~1300-1850 CE) around 1600-1850 CE (Menounos et al., 2009; Barclay et al., 2009; Hawkins et al., 2021). The timing and magnitude of the most extensive Holocene glacier expansion in the eastern Yukon and Northwest Territories, which places modern glacier retreat in context, thus remains uncertain.

The primary objectives of our study are to: i) develop a Holocene glacier chronology in the Mackenzie and Selwyn mountains of eastern Yukon and Northwest Territories and ii) use our glacier chronology to estimate changes in climate responsible for these glacier fluctuations. We then deepen our understanding of glacier activity in this area by estimating glacier volume change using multiple models of past climate to force a glacier flowline model. Finally, we briefly evaluate future glacier change in this region in response to various greenhouse gas emissions scenarios.

2 Study area

The Mackenzie and Selwyn ranges extend over 600 km from north of the Liard River in northwestern British Columbia to the Stewart River and northern extent of the Mackenzie Range in northern Yukon (Fig. 1). This region is covered by 650 km^2 of ice from nearly 1200 glaciers situated among peaks that rise as high as 2952 m above sea level (Pfeffer et al., 2014). Bedrock consists of faulted and folded Paleozoic sedimentary rocks with Early Cretaceous granitic intrusions (Pfeffer et al., 2014; Cecile and Abbott, 1989). A portion of our study area is situated in the Nahanni (Nááts'ihch'oh) National Park Reserve, which was expanded in 2009 to >30,000 km^2 (Demuth et al., 2014). Two of our nine field sites are located nearly 200 kilometers to the northwest of Nahanni National Park Reserve and are situated on or adjacent to the Keele Peak massif, which is similarly composed of Early Cretaceous granitic rock. The mean annual air temperature and average annual precipitation (1966-1990) in Tungsten, YT (61.95° N, 128.25° W, 1143 m a.s.l.) in the northern extent of Nahanni National Park is -5.1 °C and 643 mm, respectively (Env. and Climate Change Canada 2022). Storms are generally sourced from the North Pacific, though northwesterly air associated with the Arctic Low also plays an important role in the regional climate (Tomkins et al., 2008).

3 Methods

To summarize our methods, our glacier chronology originates from digitized glacier margins of aerial photos and satellite imagery, then dating late Holocene moraines using cosmogenic ^{10}Be surface exposure dating. We use this chronology to estimate paleoclimate conditions in the late Holocene using several methods. First, we estimate past and present equilibrium line altitudes (ELA) using the maximum elevation of lateral moraines (MELM, LIA maximum only), toe-to-headwall altitude ratio (THAR), and accumulation area ratio (AAR) and infer changes in temperature and precipitation (Braithwaite and Raper, 2009; Meier and Post, 1962; Ohmura and Boettcher, 2018). Then we estimate the temperature decrease needed to grow glaciers to their late Holocene positions using a flowline glacier

model. Additionally, we perturb monthly temperature and precipitation from several General Circulation Model (GCM) simulations of climate since 850 CE to produce modeled glacier extents that most closely match the terrestrial and remotely sensed record (Taylor et al., 2012) before evaluating past modelled glacier volume change for all glaciers in the Mackenzie and Selwyn mountains. Finally, we model future glacier change in this region under various

95 Representative Concentration Pathways (RCPs; Moss et al., 2010).

3.1 Field site selection

We selected sampling locations within the Mackenzie and Selwyn Mountain ranges using satellite imagery, aerial photos, and digital elevation data to identify purported late Holocene moraines. We consulted bedrock geologic maps of the area to locate sites that likely contained quartz-bearing lithologies suitable for [10]Be surface exposure dating

100 (hereafter [10]Be dating), which was then confirmed in hand-samples in the field (Cecile and Abbott, 1989; Gordey, 1992). Helicopters and floatplanes during late summer in 2014, 2016, and 2017 provided access to the field sites.

3.2 Mapping of former and present glacier extents

We manually digitized past glacier outlines for six of the nine glaciers sampled for [10]Be dating. Those glacier extents represent sites with multiple dated moraine boulders and morphologies better suited for glacier flowline modeling.

105 The resulting glaciers used in paleoclimate reconstructions are Anderson, Mordor, North Moraine Hill, Butterfly, Keele Peak, and Arrowhead glaciers (Fig. 2). Other than North Moraine Hill and Butterfly glaciers, it is the authors' understanding that the remaining glaciers in our study have no formal name. We used imagery from airphotos between 1949 and the mid-1970's CE and satellite imagery from 1985 CE, onward (SM Table 2). Air photos represent digitally scanned negatives housed at the Canadian National Airphoto Library (NAPL). We georeferenced each airphoto by

110 manually selecting 40-60 ground control points (GCPs) on the air photographs and high-resolution satellite imagery (e.g. large boulders, peaks, and ridges). We subsequently performed a thin-plate spline transformation in GIS software (QGIS), visually inspecting the georeferenced image for any obvious distortions. Portions of glacier outlines further from GCPs have positional errors smaller than 20 m.

115 We used Landsat 5, 7, and 8 satellite imagery to delineate glacier margins at roughly 5-10 year intervals from the mid-1980's onward. To aid in the manual digitization, we made false color composites for each Landsat scene to highlight the glacier surface relative to non-glaciated terrain. The surfaces of most glacier termini are debris free, which facilitated glacier mapping. We mapped late Holocene glacier margins using high resolution satellite imagery from Mapbox and PlanetLabs to delineate glacier trimlines and moraine crests. In areas with cloud cover or snow-covered

120 terrain, we used hillshades from ArcticDEM to help identify moraine ridges (Porter et al., 2018).
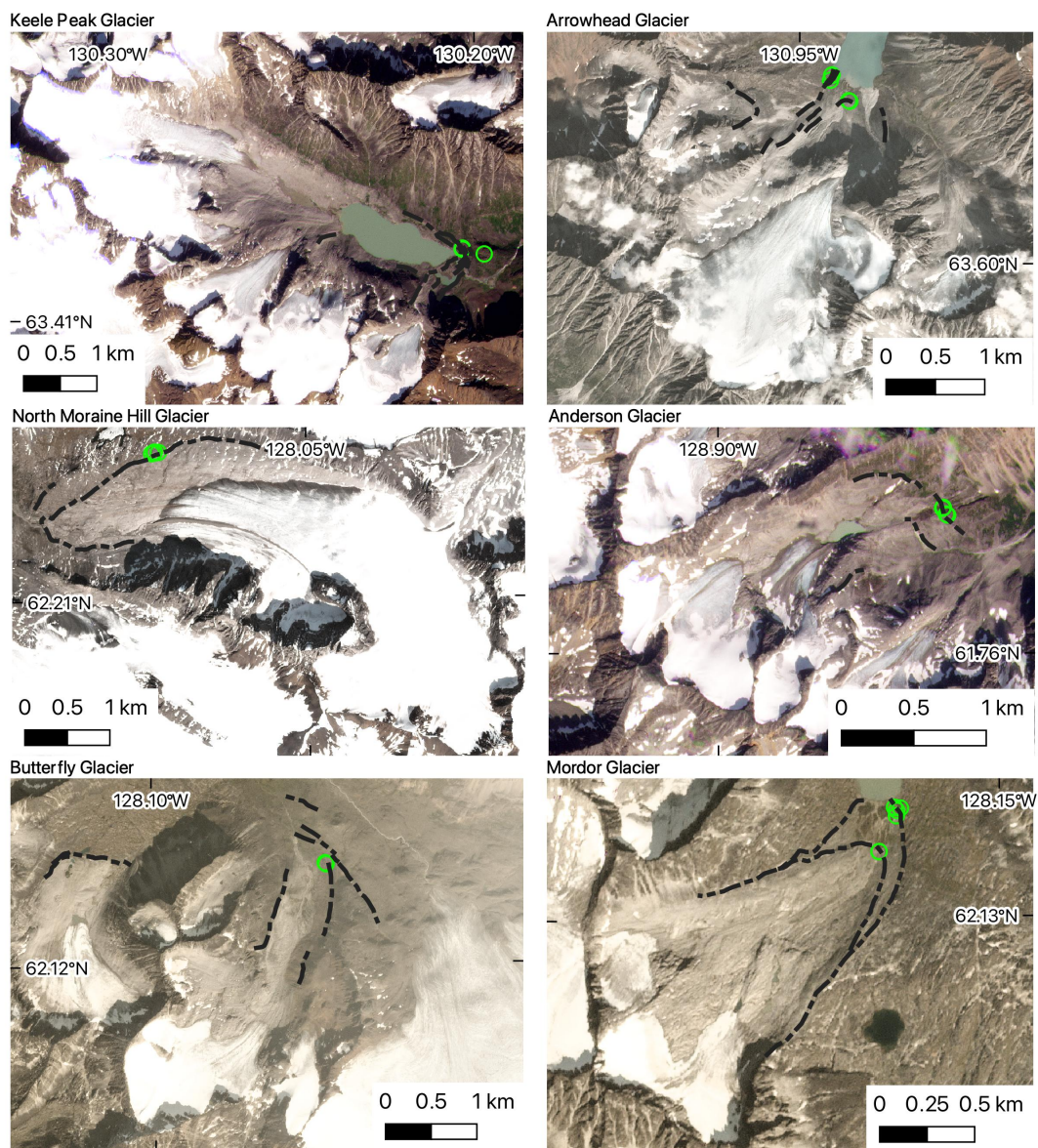
Figure 2: Glaciers from which [10]Be samples were collected. Sample locations are shown as green circles. Moraine crests are depicted as black dashed lines. Imagery is from PlanetLabs, acquired between July and August, 2021.

3.3 [10]Be field sampling

125   We targeted samples from large (generally taller than 1 m), granitic boulders on or near moraine crests (Fig. 2, SM Fig. 3). It is commonly assumed that large boulders on moraine crests are windswept such that snow cover is minimal, and their large size limits the chance of being previously covered by moraine material or moving following deposition.

Recent work by Tomkins and others (2021) provides evidence that sampling from the crests of moraines may not reduce the chance of geomorphic exposure age scatter, however at the time of sampling in this study, we followed the
130   common practice of targeting boulders on moraine crests. Several erratic boulders directly overlying bedrock and distal to the moraine crests were sampled as well (SM Data). We measured topographic shielding of the incoming cosmic ray flux and boulder self-shielding using a Brunton compass and inclinometer, and then determined the location and elevation of each sample with a handheld GPS receiver with barometric altimeter. Samples were collected from the top surfaces of boulders using a concrete saw and hammer and chisel to collect approximately 1 kg of rock.

135   ### 3.4 ^{10}Be laboratory procedures and AMS measurements

The Lamont-Doherty Earth Observatory Cosmogenic Nuclide Laboratory processed samples collected in 2014, and we analyzed the remaining samples in the Tulane University Cosmogenic Nuclide Laboratory. All samples were crushed, milled, and sieved to 250-750 μm. Physical and chemical isolation of quartz was completed following the procedures of Nichols and Goehring (2019). We isolated Be using standard chemical isolation procedures, including
140   anion and cation exchange columns (Ditchburn and Whitehead, 1994; Schaefer et al., 2009). We included a process blank with every batch of ~eight samples (SM Table 1). We sent sample aliquots of extracted Be to either the Purdue Rare Isotope Measurement (PRIME) Laboratory or the Lawrence-Livermore National Laboratory for AMS measurements, which were normalized to the standard KNSTD dilution series (Nishiizumi et al., 2007).

145   We calculated the exposure ages for all samples using version 3 of the online exposure age calculator formerly known as CRONUS-Earth, hosted by the University of Washington (https://hess.ess.washington.edu/). We used the default ^{10}Be reference production rates from the "primary" calibration dataset (Borchers et al., 2016) and report individual sample ages using the Lifton-Sato-Dunai (LSDn) scaling scheme and 1-sigma analytical errors (Table 1). Moraine ages are reported as the median exposure age ± interquartile range.

Sample	Latitude	Longitude	Elevation (m asl)	Thickness (cm)	Shielding	Quartz (g)	Carrier added (g)[a]	10Be/9Be ratio	1 sigma uncertainty	Blank-corrected 10Be conc. (atoms/g)[b]	Blank-corrected 10Be conc. uncertainty (atoms/g)	Exposure age a (LSDn)[c,d]	Exposure age uncertainty	AMS Facility
Nahanni Nat'l Park area														
Nahanni 01														
14NA-01	61.9075	-127.8688	1500	1.64	0.934	15.01	0.183	6.20E-15	5.32E-16	5.18E+03	4.45E+02	300	26	LLNL-CAMS
14NA-02	61.9075	-127.8686	1500	2.02	0.9272	15.068	0.1836	7.57E-15	5.09E-16	6.36E+03	4.27E+02	366	25	LLNL-CAMS
14NA-03	61.9079	-127.8697	1515	1.9	0.9212	14.023	0.1834	7.79E-14	1.75E-15	6.97E+04	1.53E+03	*4061*	89	LLNL-CAMS
												Median ± IQR 366 ± 940		
Nahanni 02														
14NA-04	61.8924	-127.8406	1550	1.6	0.9614	15.003	0.1828	1.36E-14	8.85E-16	1.14E+04	7.39E+02	608	39	LLNL-CAMS
14NA-06	61.8925	-127.8404	1550	2.22	0.9595	15.005	0.1827	1.52E-14	1.33E-15	1.27E+04	1.10E+03	677	59	LLNL-CAMS
												Median ± IQR 643 ± 17		
Butterfly Glacier														
14NA-07	62.1299	-128.0637	1710	2.12	0.9837	13.729	0.1833	7.02E-15	4.72E-16	6.46E+03	4.34E+02	315	21	LLNL-CAMS
14NA-09	62.1298	-128.0635	1715	1.93	0.9824	15.032	0.1833	8.88E-14	2.10E-15	7.41E+04	1.78E+03	*3637*	87	LLNL-CAMS
												Median ± IQR 1976 ± 830		
"Anderson" Glacier														
16-AND-02	61.769	-128.8705	1606	2.5	0.9656	27.207	0.2673	1.41E-14	4.76E-16	8.51E+03	3.46E+02	457	19	LLNL-CAMS
16-AND-03	61.769	-128.8706	1607	2.5	0.9653	28.24	0.2676	9.20E-15	3.88E-16	5.09E+03	2.76E+02	282	15	LLNL-CAMS
16-AND-04	61.769	-128.8706	1608	2.5	0.9656	39.269	0.2681	1.23E-12	2.29E-15	5.56E+04	1.19E+03	*3063*	66	LLNL-CAMS
16-AND-05	61.7686	-128.87	1605	2.5	0.9628	50.011	0.2672	5.50E-13	1.46E-14	1.96E+05	5.57E+03	*10874*	310	LLNL-CAMS
16-AND-06	61.7686	-128.8701	1606	2.5	0.9676	50.053	0.2674	5.64E-13	1.05E-14	2.00E+05	4.26E+03	*11038*	236	LLNL-CAMS
												Median ± IQR 457 ± 695		
"Mordor" Glacier outer moraine														
16-MOR-13	62.1301	-128.1604	1765	2.5	0.9762	37.115	0.2567	6.13E-14	1.54E-15	2.74E+04	8.21E+02	1264	38	LLNL-CAMS
16-MOR-14	62.1302	-128.1606	1764	2.5	0.9765	50.011	0.258	3.06E-14	8.47E-16	8.83E+03	4.96E+02	415	23	LLNL-CAMS
16-MOR-15	62.1298	-128.1604	1765	2.5	0.9792	50.012	0.2583	1.02E-13	1.92E-15	3.45E+04	8.67E+02	1597	40	LLNL-CAMS
16-MOR-16	62.1302	-128.16	1761	2.5	0.9769	50.016	0.2569	6.53E-13	1.53E-14	2.31E+05	5.95E+03	*11111*	287	LLNL-CAMS
												Median ± IQR 1264 ± 295		
"Mordor" Glacier inner moraine														
16-MOR-11	62.1281	-128.1622	1785	2.5	0.9754	46.672	0.2567	2.51E-14	9.34E-16	7.98E+03	4.02E+02	371	19	LLNL-CAMS
16-MOR-12	62.1281	-128.1622	1762	2.5	0.9754	50.023	0.2572	2.89E-14	8.32E-16	8.81E+03	3.47E+02	415	16	LLNL-CAMS
												Median ± IQR 393 ± 11		
North Moraine Hill Glacier														
16-MH-16	62.2256	-128.0849	1870	2.5	0.9864	50.007	0.2569	1.67E-13	3.12E-15	5.93E+04	1.27E+03	2548	54	LLNL-CAMS
16-MH-17	62.2256	-128.0844	1870	2.5	0.9861	50.002	0.2579	1.91E-13	3.65E-15	6.63E+04	1.52E+03	2867	66	LLNL-CAMS
16-MH-18	62.2257	-128.0835	1869	2.5	0.986	50.005	0.2583	5.28E-14	1.49E-15	1.68E+04	6.81E+02	693	28	LLNL-CAMS
16-MH-19	62.2257	-128.0834	1866	2.5	0.9855	50.022	0.2593	1.42E-14	7.06E-16	2.98E+03	4.57E+02	141	22	LLNL-CAMS
												Median ± IQR 1621 ± 1036		
Keele Peak area														
Keele Peak Glacier														
17-KP-01	63.4201	-130.2021	1548	2.5	0.9726	50.004	0.2587	5.47E-14	2.74E-15	1.94E+04	1.01E+03	1053	55	PRIME
17-KP-02	63.42	-130.2021	1542	2.5	0.9726	49.995	0.2588	1.73E-14	1.27E-15	5.99E+03	4.68E+02	340	27	PRIME
17-KP-03	63.42	-130.2021	1541	2.5	0.9694	48.52	0.259	2.47E-14	1.35E-15	8.91E+03	5.14E+02	495	29	PRIME
17-KP-04	63.4195	-130.1961	1602	2.5	0.9869	37.493	0.2587	4.50E-13	9.30E-15	2.16E+05	4.96E+03	*11637*	268	PRIME
												Median ± IQR 495 ± 178		
Arrowhead Glacier outer moraine														
17-AH-05	63.6162	-130.9434	1410	2.5	0.9364	40.254	0.2593	9.10E-15	9.36E-16	3.76E+03	4.32E+02	254	29	PRIME
17-AH-06	63.6166	-130.9432	1408	2.5	0.9364	44.016	0.2584	1.54E-14	1.18E-15	6.02E+03	4.94E+02	394	32	PRIME
17-AH-07	63.6166	-130.9431	1413	2.5	0.9364	30.637	0.2593	1.27E-14	1.04E-15	7.08E+03	6.27E+02	456	40	PRIME
												Median ± IQR 394 ± 50		
Arrowhead Glacier inner moraine														
17-AH-08	63.6143	-130.9396	1440	2.5	0.9517	50	0.2595	4.90E-15	7.40E-16	1.51E+03	2.79E+02	106	20	PRIME
17-AH-09	63.6143	-130.9393	1440	2.5	0.9517	47.738	0.2594	8.66E-15	8.22E-16	3.01E+03	3.23E+02	201	22	PRIME
												Median ± IQR 153 ± 24		

[a] Be Carrier for samples 14-NA* was 1038.3 ug/g, except samples 14-NA(02&07), whose carrier was 1038.8 ug/g. All remaining samples used a PRIME Be carrier with concentration of 1040 ppm.
[b] Isotopic ratios were meaured at either the Lawrence Livermore National Laboratory - Center for Accelerator Mass Spectrometry (LLNL-CAMS) or the Purdue Rare Isotope Measurement Laboratory (PRIME). Be-10/Be-9 ratios are not corrected for Be-10 detected in procedural blanks.
[c] Ages are calculated using version 3 of the online exposure age calculator formerly known as the CRONUS-Earth online exposure age calculator found at https://hess.ess.washington.edu/ (wrapper 3.0.2, muons: 1A, constants as of: 2020-08-26). All ages are calculated using the Lifton-Sato-Dunai "LSDn" scaling and the default production rate.
[d] The median exposure age and interquartile range (IQR) excludes the exposure age of erratics, whose age is listed in italics.

150

Table 1: ¹⁰Be sample information for all boulders sampled in this study. Median and interquartile range calculations exclude erratic boulders sampled outside of moraine boundaries.

3.5 ELA reconstructions

Variations in the equilibrium line altitude of a glacier relate to long term changes in climate. Such variations have

155 been used to estimate changes in either temperature or precipitation (Dahl and Nesje, 1992; Moore et al., 2022; Oien et al., 2022). Commonly used methods to reconstruct past ELA's include the maximum elevation of lateral moraines, toe-to-headwall altitude ratio, and accumulation area ratio, among others. Each method offers advantages and limitations in reconstructing past ELA's (Benn et al., 2005; Nesje, 1992; Porter, 2001; Osmaston, 2005). We use the

MELM, THAR, and AAR methods of ELA reconstruction to estimate glacier ELAs between the Little Ice Age (ca.
160   1300-1850 CE) and modern time (2000-2021 CE).

To record the MELM for each glacier, we used high resolution satellite imagery and elevation data from ASTER
GDEM version 3 to identify the highest elevation of preserved lateral moraines.

165   The THAR method assumes a glacier's ELA is positioned at a fixed ratio between the maximum and minimum
elevation of the glacier, shown in Eq. (1):

$$ELA \ = \ minimum \ glacier \ elevation \ + \ (glacier \ elevation \ range \ \times \ THAR) \tag{1}$$

Work by Meirding (1982) and Murray & Locke (1989) found that ratios of 0.35 to 0.4 yielded satisfactory estimates
of alpine glacier ELA's. Here, we use the mean ELA from a THAR of 0.35 and 0.4.

170

The accumulation area ratio assumes a fixed ratio of the accumulation area to the total area of a glacier in equilibrium
(Braithwaite and Raper, 2009; Meier and Post, 1962). Here, we assume the AAR for glaciers in this region to be 0.6,
which is generally considered to be the ratio of steady state cirque and valley glaciers in NW North America (Porter,
1975).

175

We generated LIA and modern glacier hypsometries by clipping ASTER GDEM version 3, 30 m resolution digital
elevation data to the digitized glacier extents. The modern DEM does not account for the paleo surface of the glacier
during the LIA and may negatively bias the paleo-ELA (Porter, 2001).

180   For each ELA reconstruction method, we inferred the change in average temperature (dT) from the Little Ice Age to
present as a function of changing ELA by assuming an environmental lapse rate of -6.5 °C km^{-1}.

The ELA of a glacier is also influenced by changes in precipitation. Ohmura et al. (2018; 1992) empirically derive an
equation (Eq. 2) to estimate the annual precipitation, P, in millimeters water equivalent (mm w.e.) at the ELA of a
185   glacier, given a mean summer (JJA) temperature T:

$$P \ = \ a \ + \ bT \ + cT^2, \tag{2}$$

where, a = 966, b = 230, and c = 5.87. We estimated changes in precipitation at the ELA of each study glacier by
assuming a modern (1986-2015 CE mean) JJA temperature (T) at the modern ELA from the fifth generation European
Centre for Medium-Range Weather Forecasts (ECMWF) global climate atmospheric reanalysis (ERA5). We use our
190   dT estimate from our ELA reconstructions to yield Eq. 3:

$$P_{LIA} \ = \ a \ + \ b(T-dT) \ + \ c(T-dT)^2 \tag{3}$$

We selected ERA5 2 m surface temperatures (Hersbach et al., 2020) from the grid cell nearest to the study glacier and
used the same -6.5 °C km^{-1} lapse rate to approximate T at the modern ELA.

3.6 Glacier modeling

195 **3.6.1 Open Global Glacier Model**

Our final method of ELA reconstruction used the Open Global Glacier Model (OGGM; Maussion et al., 2019) which is a modular, open-source model framework with the capacity to model glacier evolution for all glaciers on Earth. The glacier model within OGGM is a depth-integrated flowline model that solves the continuity equation for ice using the shallow ice approximation (Cuffey and Paterson, 2010). Multiple flowlines for each glacier are calculated using a

200 DEM clipped around the glacier polygon using the routing algorithm of Kienholz et al. (2014). The default mass-balance model used in OGGM begins with gridded monthly climate data, here the Climatic Research Unit gridded Time Series (CRU TS) version 4.04 (Harris et al., 2020). The climate data feeds a temperature index model described in Marzeion et al. (2012), incorporating a temperature sensitivity parameter that is calibrated using nearby glaciers with observations of specific mass balance (Zemp et al., 2021). Ice thickness is estimated by assuming a given glacier

205 bed shape (parabolic, rectangular, or mixed) and applying a mass-conservation approach that employs the shallow-ice approximation. OGGM assumes that the "modern" glacier outline, sourced from the Randolph Glacier Inventory (RGI), is from the same date as the DEM. Users are also able to supply their own glacier outlines. More information on OGGM can be found on OGGM.org, or in publications on the model (Maussion et al., 2019; Eis et al., 2021).

210 **3.6.2 Equilibrium run**

In our first experiment using OGGM, we started with the RGI polygons for the six of our study glaciers targeted for surface exposure dating (Anderson, Mordor, Butterfly, North Moraine Hill, Keele Peak, and Arrowhead glaciers). We then ran a 1000-year simulation under a constant climate, iteratively adjusting a temperature bias relative to the average CRU TS climate centered around 2000 CE (close to the RGI polygon date of most glaciers in the region) until

215 the modeled glacier reached equilibrium at or very near the glacier length indicated by the moraine record. From these equilibrium run experiments, we produce three different estimates of ELA and temperature change. First, the temperature lowering required to expand a glacier to its LIA length was interpreted as the approximate temperature change from the LIA to 2000 CE. Second, we then extracted the hypsometry of the modeled glacier at t=0 (modern extent) and t=1000 (LIA extent) and estimated the modeled ELA using the same AAR method as described in section

220 3.5, again assuming an AAR of 0.6. We can again apply the -6.5 °C km^{-1} lapse rate to estimate the apparent temperature change from modelled glacier extents between the two time periods. Third, for the modern glacier extent, we extracted the elevation at which the modeled surface mass balance of each glacier is equal to zero without any temperature bias. This represents the modern *climatic* ELA and is not based on glacier morphology.

3.6.3 Transient run

225   In our next experiment with OGGM, we simulate changes in glacier volume in the Mackenzie and Selwyn mountains using our glacier chronology to tune the climate model input. We used OGGM to simulate the response of our five glaciers driven by monthly temperature and precipitation variability from four Coupled Model Intercomparison Project Phase 5 (CMIP5) GCM runs (CCSM4, MIROC-ESM, MPI-ESM-P, and MRI-ESM2; Taylor et al., 2012). All GCMs incorporate volcanic, total solar irradiance, summer insolation in both hemispheres, aerosol and greenhouse

230   gas emission, and land use change forcings over the period 850-2005 CE (Landrum et al., 2013; Sueyoshi et al., 2013; Yukimoto et al., 2019).

We omitted the glacier on Keele Peak, as its RGI outline includes several cirque glaciers separated from the main glacier, which causes OGGM to produce a problematic flowline that crosses several flow divides. We set the mass

235   balance gradient for each glacier to 5.2 mm w.e. m^{-1} based on the mass balance gradient for Bologna Glacier in Nahanni National Park Reserve for the 2014-2015 CE balance year (Ednie and Demuth, 2019). For each GCM, we ran 300-500 simulations incrementally perturbing the temperature bias (Tbias) and precipitation factor (Pbias) to determine which combination of temperature and precipitation bias produces a modeled glacier length time series that best fits our glacier chronology. For each simulation, we calculated the summed root mean squared error (RMSE) of

240   modeled glacier length versus the moraine and remotely sensed glacier length at multiple timesteps. The combination of Tbias and Pbias that produced the lowest RMSE was selected as the "optimized" set of parameters for each glacier and GCM.

Finally, we averaged the set of Tbias and Pbias from each glacier that produced the lowest RMSE for each GCM and

245   applied those corrections before running simulations of the past millennium for all (1235) glaciers in the eastern YT/NWT, forced by each "calibrated" GCM. We then compared the modeled glacier volume change over the past millennium to our chronology as well as what is already known about late Holocene glacier change in this region to evaluate if the modeling results were reasonable.

3.6.4 Future glacier simulations

250   Finally, we use OGGM to project 21st-century glacier change for all 1235 glaciers in the eastern Yukon and Northwest Territories, forced by four different CCSM4 projection runs under different representative concentration pathways (RCPs). We use the default model parameters of OGGM v1.5.3 and rely on OGGM's pre-processed glacier directories, which already contain glacier geometry and climate data.

255   The historical climate data is CRU TS version 4.04 (Harris et al., 2020). We then download the CMIP5 (CCSM4) climate model output from four different RCP's and run OGGM's bias correction against the CRU calibration data, which in turn calculates anomalies from the CRU reference climatology (1961-1990 CE). Finally, we run OGGM for

all 1235 glaciers forced by the calibrated climate scenarios from 2020 to 2100 CE and analyze the projected change in glacier area and volume.

4 Results

4.1 Glacier chronology

Glaciers in the Mackenzie and Selwyn mountains deposited moraines fronting cirque and valley glaciers 0.7 to 2 km beyond their ca. 2020 CE extents. These moraines are typically devoid of vegetation other than widespread lichen cover. The moraines we sampled are commonly boulder-rich, with pebble-cobble matrices (SM Data).

Many alpine cirques preserve two nested moraines within tens of meters of each other. We observed nested moraine crests at Keele Peak, Arrowhead, North Moraine Hill, and Mordor glaciers. There is also a partially-nested crest preserved at Anderson Glacier. We did not sample both crests at most locations since our focus was to date the outermost moraines.

Erratic boulders 10-40 m beyond cirque moraines at Anderson and Mordor glaciers date to 10.9-11.1 ka (Table 1). An erratic sampled ~250 m beyond the late Holocene moraine fronting Keele Peak glacier dates to 11.6 ± 0.3 ka. Erratic boulders directly overlaid bedrock and had abundant lichen cover. We did not observe any obvious signs of boulder surface erosion, such as grüssification, solution pitting, or enhanced relief of resistant minerals.

In the Nahanni National Park region, the median ^{10}Be age on moraine boulders is 610 ± 850 a (ca. 1405 CE, n = 19). Adjacent to Keele Peak, the median moraine exposure age is 370 ± 110 a (ca. 1650 CE, n = 8). Together, the sampled moraines in this study date to 460 ± 415 a (ca. 1560 CE). We sampled both the inner and outer crest of the moraine couplet at Arrowhead and Mordor glaciers. At Anderson Glacier, the outer moraine dates to 390 ± 50 a (1620 CE, n = 3) and the inner moraine to 150 ± 24 a (1860 CE, n = 2). At Mordor Glacier, the outer moraine dates to 1260 ± 295 a (760 CE, n = 3) and the inner moraine dates to 390 ± 22 a (1630 CE, n = 2).

There is notable scatter in the exposure ages on many of the sampled moraines (Table 1, Fig. 3). At Nahanni 01, Butterfly, Anderson, Mordor, and North Moraine Hill glaciers, there is at least one sample from each moraine that returned ages older than 1 ka. This scatter gives individual moraine ages large errors, however when we analyze all moraine boulder ages together, there is a distinct peak in exposure ages between ~800 to 100 a exposure (ca. 1200 to 1900 CE), with the greatest peak around 480 to 280 a (1540-1740 CE, Fig. 3).
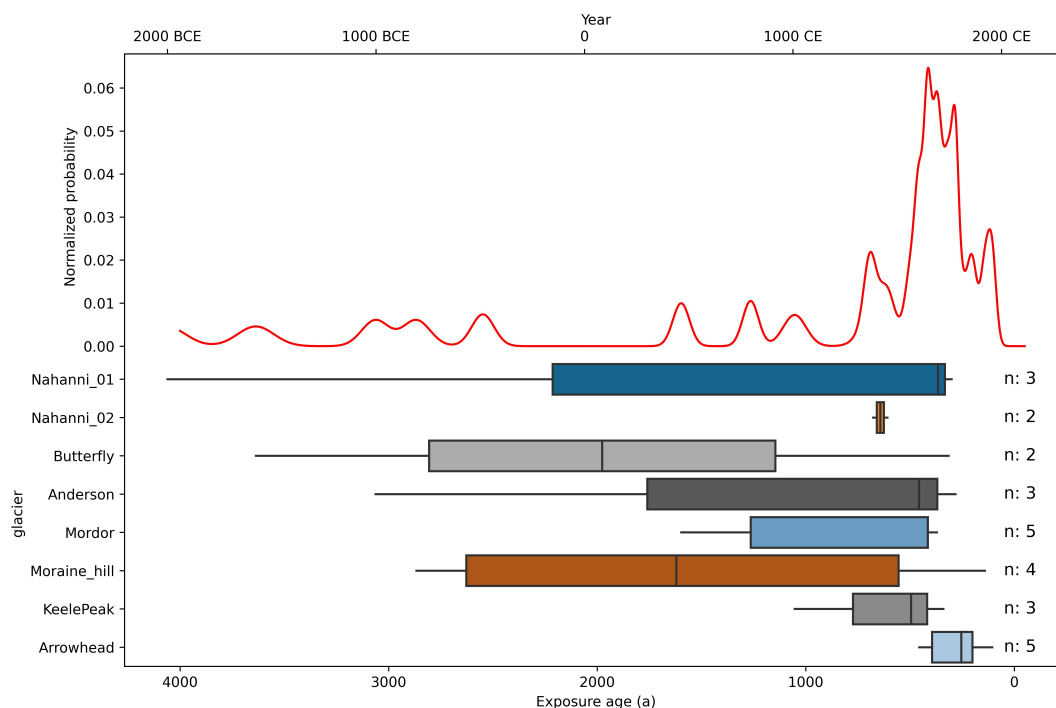
Figure 3: Box and whisker plots of ¹⁰Be surface exposure ages for each glacier, showing the interquartile range and median age of each moraine surface and the normalized probability density function (red line) for all ¹⁰Be samples.

4.2 Climate reconstructions since the late Holocene

ELA reconstruction using the different methods described above yield a range of estimated changes in ELA between the LIA and modern time (Fig. 4). We use ELA's from the AAR method using mapped former and modern glacier extents as the "standard" ELA against which we compare our other ELA estimates. Any ELA reconstruction method could serve as the "standard", however the AAR method was selected due to its common usage in glacier reconstructions. When comparing ELA change within a single method, "dELA" is the change in reconstructed ELA between the LIA and modern time using the method in question. As discussed more below, we assume that precipitation remains constant between the LIA and modern time for ELA reconstructions using the MELM, THAR, and AAR methods.
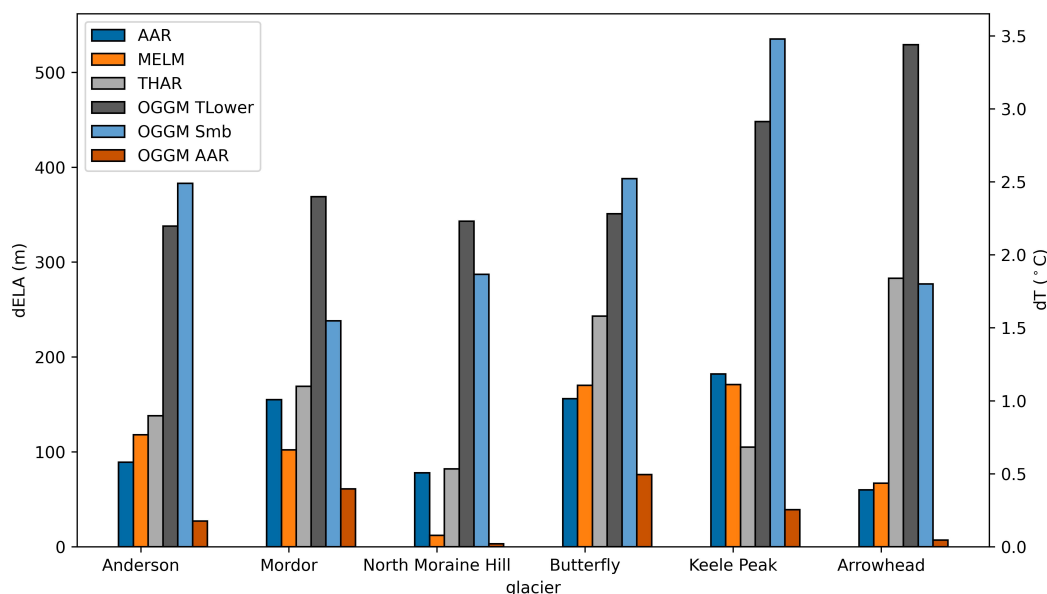
300

Figure 4: Changes in ELA and estimated temperature change between the Little Ice Age maximum to modern (ca. 2015) for six glaciers in this study. Each method used for reconstruction is discussed in text.

The modern ELA derived from the AAR method is +12 m to +171 m (average 107 m) higher than the LIA ELA using

305 the maximum elevation of lateral moraines method, corresponding to a +0.1 to +1.1 °C (average 0.9 °C) increase in temperature (Fig. 4). Using the THAR method, the dELA's range from +47 m to +240 m (average 138 m), corresponding to a dT of +0.3 to +1.6 °C (average 0.9 °C) since the LIA.

ELA's reconstructed from LIA and modern glacier extent mapping, assuming an AAR of 0.6, indicate a rise in ELA

310 since the LIA of +60 to +182 m, corresponding to a +0.4 to +1.2 °C (average 0.8 °C) increase in annual average temperature (Fig. 4).

Using OGGM, we include three estimates of ELA change. Non-transient simulations on glaciers in the Nahanni National Park region using OGGM require +2.3 °C of warming, relative to the 30-yr average climate centered around

315 2000 CE, to retreat from their LIA extents to modern positions. Keele Peak and Arrowhead glaciers require nearly +3.2 °C average warming since the LIA relative to their modern temperature (Fig. 4). This warming is equivalent to a dELA since the LIA of +354 m in Nahanni National Park and +492 m in the Keele Peak area.

Applying the AAR method, but with OGGM-derived glacier hypsometries at the LIA and modern time, indicates

320 much less warming since the LIA, with rises in ELAs between +7 m and +76 m, corresponding to a rise in temperature of <0.1 to 0.5 °C. We interpret this minimal change in ELA to be the result of glacier surface thickening in the OGGM

model when the glacier expands to LIA extents, which reduces the apparent ELA change as the lower portion of the modeled glacier surface thickens (SM Fig. 5 & 6).

325 The third variation of ELA reconstruction using OGGM estimates the modern ELA not from modeled glacier hypsometry, but rather the elevation at which the modeled surface mass balance on the glacier is equal to zero. In a warming climate, this estimate of glacier ELA is expected to be higher than the AAR-derived ELA, as a glacier undergoing rapid retreat has a morphometry that lags behind the climate signal. Changes in ELA using the modern mass balance-derived ELA and the AAR-derived LIA ELA range from +277 m to +535 m. Estimated temperature
330 change indicates a rise in temperature since the LIA of +1.6-3.5 °C.

Using the equation of Ohmura et al. (2018) and temperature change estimates from our AAR-derived ELAs, we estimate that compared to modern values, there was -117 to -339 mm w.e. yr^{-1}, or 5-15% (average 10%), less precipitation at the ELA of our study glaciers during the LIA (SM Table 3).

335 **4.3 Past millennium glacier change**

Estimates of glacier evolution in the YT and NWT over the past millennium vary among the four GCMs (Fig. 5). The MPI simulation shows steady glacier volume until 1600 CE, while MRI, MIROC, and CCSM4 indicate a reduction in glacier volume until ca. 1250 CE, afterwards CCSM4 and MRI (and to a lesser degree MPI) show an increase in glacier volume until ca. 1400 CE before a period of stable ice volume until ca. 1600 CE. MRI, MPI and CCSM4 all
340 indicate glacier expansion ca. 1600 CE, with MPI reaching a maximum ice volume of 38.1 km^3 at 1765 CE and CCSM4 producing a maximum ice volume of 34.7 km^3 at 1855 CE (Fig. 5). MRI appears to largely miss 20th century glacier retreat and continues to show glacier expansion until 1980 CE, followed by volume loss. Glacier volume simulated by MIROC decreases through the past millennium, in contrast to the other GCM simulations. Projections of future glacier loss (below) using CCSM4 climate simulations begin with an initial regional ice volume of 18.1 km^3
345 in 2019 CE. Compared to the maximum modeled ice volume in the CCSM4 past millennium simulations, this represents a 48% loss in ice volume since ca. 1850 CE.
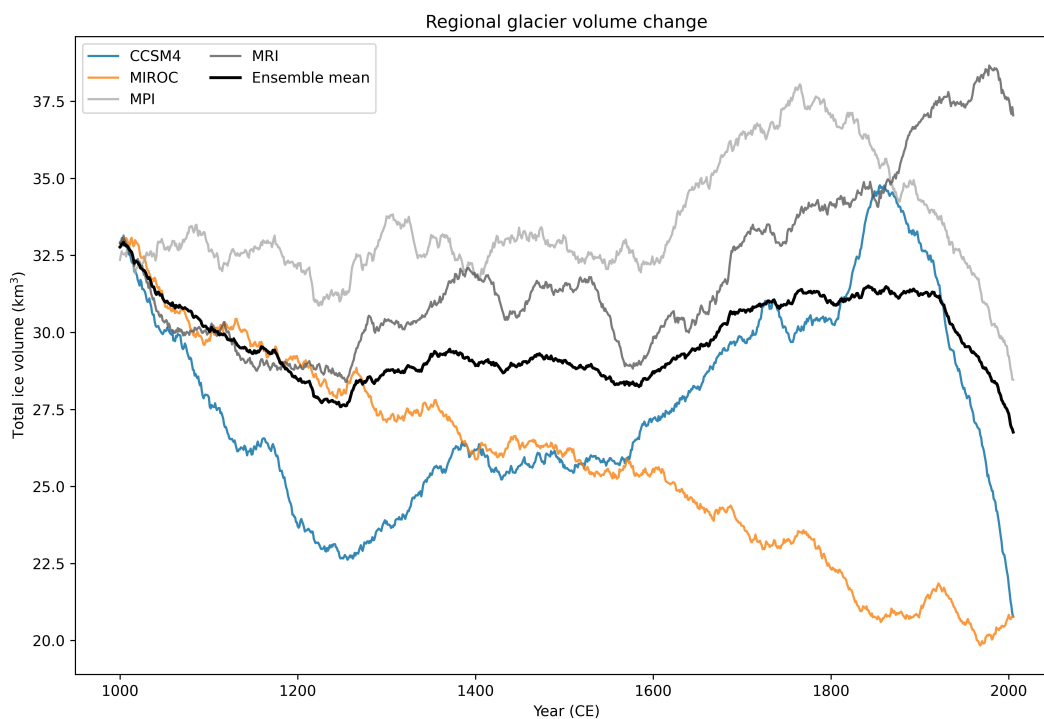
Figure 5: Modeled ice volume change for all glaciers in the eastern YT and NWT produced by OGGM using four different GCMs.

4.4 21st Century glacier projections

Under all CCSM4 21st century emissions scenarios, glacier volume in the eastern YT and NWT significantly declines throughout this century (Fig. 6). Glacier volume is projected to decrease by 85% under RCP2.6 and 97% under RCP8.5, compared to 2019 CE values. The greatest rate of ice loss is projected to be between present day and ca. 2040 CE, then the rate of volume decline slowly decreases through to the end of the century.
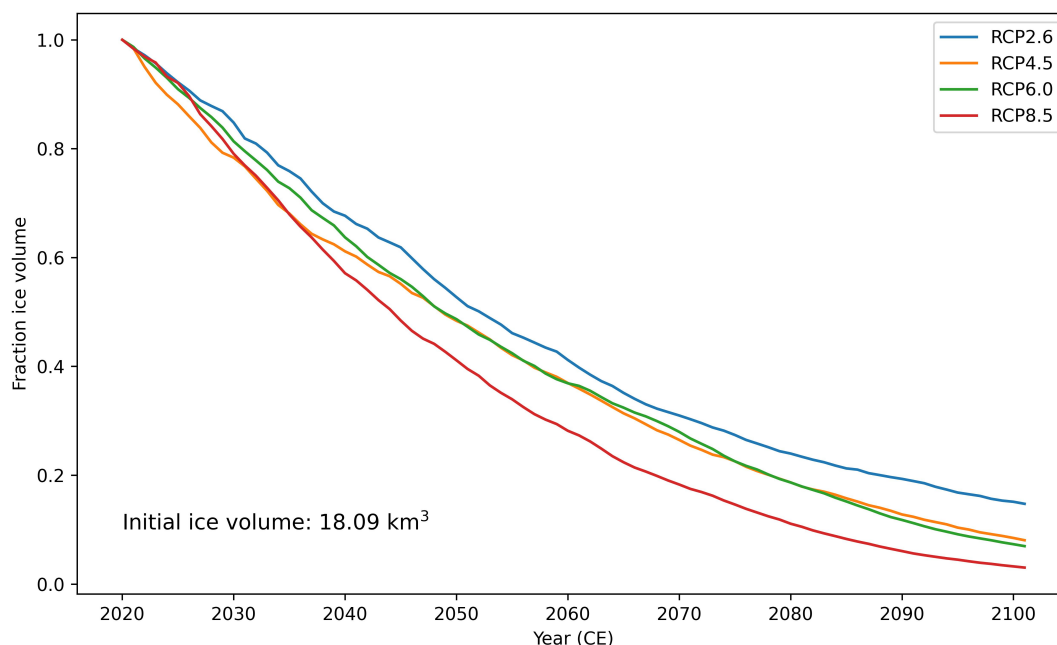
Figure 6: **Fractional glacier volume change until 2100 CE under various representative concentration pathways (RCPs) for all glaciers in the eastern YT and NWT.**

5 Discussion

5.1 Holocene glacier fluctuations

Early Holocene erratic boulders just beyond moraines dating to the last millennium, as well as a lack of moraines down valley of the latest Holocene moraines, implies that since ca. 11 ka, glaciers in this region were no more extensive than during the latest Holocene. These results accord with records from southern Alaska and western Canada (Menounos et al., 2009; Mood and Smith, 2015; Barclay et al., 2009), as well as in Europe (Braumann et al., 2020, 2021; Ivy-Ochs et al., 2009) that show most alpine glaciers within these regions reached their greatest Holocene positions during the last several hundred years. We interpret the erratic boulders to record local deglaciation associated with the termination of the Younger Dryas cold interval (Menounos et al., 2017; Seguinot et al., 2016; Braumann et al., 2022).

Our moraine chronology generally accords with the limited previous work in this region. Moraine ages from this study suggest glaciers reached their LIA maximum closer to 1560 CE, with a possible readvance or standstill in the mid-1800's. Tomkins et al. (2008) used varve and tree ring records near Tungsten, YT to infer periods of glacier growth around the late 1300s to 1450 CE, 1600 to 1670 CE, 1730 to 1778 CE, and an apparent Little Ice Age maximum 1778-1892 CE. Dyke (1990) completed an extensive lichenometric survey of rock glaciers and late Holocene moraines

375 directly west and south of Tungsten, dating most late Holocene moraines to within the past 400 years. Our moraine chronology is in general agreement with the lichenometric ages of Dyke (1990) and suggests an earlier Little Ice Age maximum than interpreted by Tomkins et al. (2008). The significant scatter in our [10]Be moraine dataset complicates our interpretations of decadal-to-century scale glacier fluctuations, however.

5.2 ELA and climate reconstruction

380 In this study, we reconstructed and estimated past and present glacier ELA's through several methods, inline with recommendations by Benn et al. (2005) that multiple ELA reconstruction methods be used to provide a more robust estimation of past ELA's and uncertainty with each reconstruction method. An important limitation to the AAR and THAR method is that it does not account for modern glaciers being out of equilibrium with modern climate. If the modern ELA is not accurately known and the glacier is retreating or advancing in response to climate perturbations, 385 then comparisons in ELA change between modern and other time periods will under- or over-estimate ELA departures (Porter, 2001). Additionally, the assumption that a glacier's ELA only fluctuates due to changes in temperature is an oversimplification (Ohmura et al., 1992). Increased (decreased) precipitation will lead to a higher (lower) mass balance and may obscure the impact of temperature change on glacier response (i.e. Shea et al., 2004).

Anderson et al. (2011) presents lacustrine $\delta^{18}O$ records from the central Yukon that suggest a wet, early Little Ice Age, 390 then dry conditions until modern day, in response to the changing position and strength of the Aleutian Low. If glaciers in the Mackenzie and Selwyn Mountains received greater snowfall during the LIA, then less cooling would be needed to grow glaciers to their LIA extents. Tomkins et al. (2008) developed a July mean temperature reconstruction from tree rings and varved lake sediments close to Tungsten, near the northern end of Nahanni National Park Reserve. Their amalgamated temperature reconstruction demonstrates the differing signals of varved lacustrine sediment and tree 395 ring records, but does suggest cooler temperatures in the early 1800's, a warm interval at the end of the 1800's to early 1900's, followed by cooling until at least the 1940's before warmer than average July temperatures until modern time.

Our non-transient experiment using OGGM provides another estimate for temperature change since the LIA, though it still ignores the effect of precipitation variability. By determining the temperature lowering from the present climate 400 needed to grow a modeled glacier to LIA extents, we remove the likely erroneous estimation of the modern glacier ELA based on current glacier hypsometry and more directly compare modern temperatures with the inferred temperature during the LIA maximum, when the glacier was in equilibrium with climate. Both the non-transient ("OGGM TLower" in Fig. 4) and surface mass balance ("OGGM Smb" in Fig. 4) incorporate modern climatology and as a result indicate generally greater temperature change since the LIA compared to glacier geometry-based 405 reconstruction methods. A bedrock borehole temperature reconstruction (62.47° N, 129.22° W) between Nahanni National Park and Keele Peak indicates around +3 °C of surface warming since 1500 CE (Huang et al., 2000), consistent with our temperature change estimates comparing past ELAs to modern climatology. In summary, we

recommend that when *in situ* mass balance measurements are not available to determine the modern ELA of a glacier, that modeled ELA's using modern climate be used to estimate present ELA's.

410

OGGM is built to perform best at regional to global scales and may produce problematic results at the scale of individual glaciers (Maussion et al., 2019). Differences between the year of DEM acquisition and RGI glacier extent, erroneous glacier margins, and lack of nearby mass balance calibration information can all have significant impacts on the evolution of individual modeled glaciers. To help give confidence that the modeling results from OGGM were

415 producing reasonable glacier evolution, we ran a simple flowline glacier model modified from Jarosch et al. (2013), which was able to grow glaciers to similar extents as OGGM (SM Fig. 2). The similar glacier evolution between the two models indicates that modeled glacier response is the result of climate inputs, rather than unique properties of each model.

420 Regular mass balance data from *in situ* mass balance measurements or remote sensing on glaciers in remote areas will help improve the performance of global glacier models like OGGM (Eis et al., 2021). A similar study design as is presented in this paper may be successfully implemented in areas with robust glacier chronologies from the late Holocene to present from many more glaciers than are included in our study. Well-constrained glacier chronologies would serve to extend the calibration or validation dataset for large scale glacier modeling efforts (i.e. Rounce et al.,

425 2023).

5.3 GCM evaluation

Of the four different CMIP5 GCM simulations tested, glacier model runs forced by CCSM4 and MPI yield glacier fluctuations that best match our general understanding of latest Holocene glacier expansion and glacier retreat over the past millennium (Menounos et al., 2009; Luckman, 2000; Figure 5). We consider the results from MRI to be

430 unreasonable due to the continued ice expansion through most of the 20th century, and similarly discount the results from MIROC due to the modeled steady glacier volume decline over the entire past millennium.

Our [10]Be chronology suggests glacier advance and moraine formation earlier than what the modeling results show. At Arrowhead Glacier, the outer and inner moraine [10]Be ages (1620 and 1860 CE, respectively) are comparable with the

435 modeled glacier evolution under the CCSM4 climate, however. MRI suggests a period of glacier retreat shortly before 1600 CE, which is consistent with our moraine chronology, however MRI, CCSM4, and MPI all suggest further ice expansion which would have overridden previously deposited moraines. If the exposure age of a moraine is interpreted to more closely record the onset of glacier retreat, rather than advance, then our moraine chronology further indicates that glaciers reached their LIA maximum extents prior to when OGGM suggests.

440

The four GCMs used in our study simulate varied temperature and precipitation time series over the past millennium, which results in differing modeled glacier responses (SM Fig. 8-11). Modeled glaciers forced by CCSM4 and MPI

reach late Holocene maxima between 1765 and 1860 CE, coincident with other late Holocene glacier records (Menounos et al., 2009; Barclay et al., 2009; Mood and Smith, 2015). Our moraine and remote sensing record allowed

445   for four GCM's to be calibrated for a small selection of glaciers in the region prior to being run for all 1235 glaciers. Without a well-dated moraine chronology, we would be unable to assess how to model performs beyond the remote sensing record.

Further research is needed to evaluate why the existing GCM simulations fail to grow glaciers at the same time as our

450   moraine chronology suggests in northwestern Canada. The moraine record offers an important method of validating glacier models beyond the remote sensing record, however moraine chronologies must be tightly constrained in order to confidently evaluate model results. Additional cosmogenic surface exposure dating in this region, especially in areas where there is an unambiguous lack of post-depositional movement may help to produce moraine chronologies with less scatter. Measuring multiple nuclides on moraine boulders (such as using paired ^{14}C/^{10}Be) would allow

455   potential inheritance to be investigated (i.e. Goehring et al., 2022). Finally, as mentioned above, consistent mass balance records from glaciers in this region would help to better constrain the influence of local climate on glacier response in the Mackenzie and Selwyn Mountains (Pelto et al., 2019; Ednie and Demuth, 2019).

5.4 Future response of glaciers to climate change

The Mackenzie and Selwyn mountains are almost certain to experience profound glacier mass loss throughout the

460   21st century. The estimated magnitude of ice volume decline agrees with modeling results by Clarke et al. (2015) who estimate a 70-95% reduction in glacier volume in the Canadian Rocky Mountains by 2100 CE. Additionally, recent work by Rounce et al. (2023) estimates 93-100% deglaciation in the Mackenzie and Selwyn Mountains by 2100 CE, depending on the magnitude of global temperature change. Under SSP3.7 and SSP5.85, this region is predicted to be fully deglaciated by 2080 CE (Rounce et al., 2023). By 2019 CE, approximately half of the ice volume was lost in the

465   Mackenzie and Selwyn Mountains in the CCSM4 run compared to the glacier maximum in 1860 CE (Fig. 5).

6 Conclusions

Based on geomorphic mapping, surface exposure ages, and numerical modeling, the following conclusions can be drawn from our study. (1) The probability distribution of ^{10}Be ages suggests that most glaciers in eastern YT and NWT reached their greatest Holocene extents during the latter half of the Little Ice Age [1600-1850 CE]; (2) the uncertainty

470   ascribed to some moraines is high, given the presence of some boulders that yielded ^{10}Be ages that predate the Little Ice Age, and future work utilizing multi-nuclide approaches would allow this scatter to be further investigated; (3) We find no evidence of glaciers extending beyond LIA limits since at least 10.9-11.6 ka, in accord with most other Holocene glacier records in the Northern Hemisphere; (4) Our ELA reconstructions suggest warming of 0.2-2.3 °C since the LIA, with morphology-based ELA reconstructions likely underestimating the modern ELA of glaciers

475   undergoing retreat; and (5) Projections of future glacier change estimate a further 85-97% loss of glacier volume in the Mackenzie and Selwyn mountains by 2100 CE, in agreement with recent global modeling efforts.

Glacier chronologies from late Holocene glacier fluctuations can provide important sources of validation of GCM simulations beyond the instrumental record, especially given the variety between individual GCM simulations of past

480   climate. Nearby *in situ* mass balance records and well-constrained late Holocene glacier chronologies are needed to help validate past millennium GCM simulations and highlight important feedbacks between the arctic and the global climate system. Modern tropospheric warming will continue to dramatically reduce glacier volume in this region, with significant impacts to the local ecosystem that relies on glacier-fed rivers and streams through the summer months.

485

Author Contributions. Author contributions follow the CRediT Authorship Guidelines.

Author:	AH	BM	BG	GO	BP	CD	JS
Conceptualization	X	X		X			X
Data Curation	X	X			X		
Formal Analysis	X	X	X				
Funding Acquisition	X	X					X
Investigation	X	X	X	X		X	X
Methodology	X	X			X		
Administration	X	X					
Resources		X	X				
Software	X	X			X		
Supervision		X	X	X			
Validation	X	X	X				
Visualization	X					X	
Original Draft	X	X					
Review/editing	X	X	X	X		X	

Competing Interests.

490 The authors declare that they have no conflict of interest.

Acknowledgements.

Funding for this study was provided by a NSERC Northern Discovery grant to BM, and a GSA Quaternary Geology and Geomorphology Division Arthur D. Howard Research Award to AH. Additional travel support was provided to

495 AH by the University of Northern British Columbia. The Geological Survey of Canada shared helicopter access in the Nahanni National Park Reserve (NNPR) and graciously allowed us use of their concrete saw. The friendly staff at the Whitehorse Airphoto Library provided invaluable assistance with field site reconnaissance. We are grateful to the Dehcho, Denendeh, and Nahanni Butte First Nations for access to complete our study on their traditional territories. Rebecca Lerch assisted in field work in NNPR. Expert flying by Alpine Aviation provided floatplane access to remote

500 sites around Keele Peak and in NNPR.

Code and data availability.

All data described in this paper that have not already been published elsewhere are included within the main text and/or supplementary materials. Code used for glacier modelling has been sourced from OGGM.org or from Jarosch

505 et al. (2013). In the event of paper acceptance and publication, the code will be posted on a publicly available repository under an open-source license.

References

510   Anderson, L., Finney, B. P., and Shapley, M. D.: Lake carbonate-δ18O records from the Yukon Territory, Canada: Little Ice Age moisture variability and patterns, Quat. Sci. Rev., 30, 887–898, 2011.

Badding, M. E., Briner, J. P., and Kaufman, D. S.: ^{10}Be ages of late Pleistocene deglaciation and Neoglaciation in the north-central Brooks Range, Arctic Alaska, J. Quat. Sci., 28, 95–102, 2013.

Barclay, D. J., Wiles, G. C., and Calkin, P. E.: Holocene glacier fluctuations in Alaska, Quat. Sci. Rev., 28, 2034–
515   2048, 2009.

Benn, D. I., Owen, L. A., Osmaston, H. A., Seltzer, G. O., Porter, S. C., and Mark, B.: Reconstruction of equilibrium-line altitudes for tropical and sub-tropical glaciers, Quat. Int., 138-139, 8–21, 2005.

Borchers, B., Marrero, S., Balco, G., Caffee, M., Goehring, B., Lifton, N., Nishiizumi, K., Phillips, F., Schaefer, J., and Stone, J.: Geological calibration of spallation production rates in the CRONUS-Earth project, Quat.
520   Geochronol., 31, 188–198, 2016.

Braithwaite, R. J. and Raper, S. C. B.: Estimating equilibrium-line altitude (ELA) from glacier inventory data, Ann. Glaciol., 50, 127–132, 2009.

Braumann, S. M., Schaefer, J. M., Neuhuber, S. M., Reitner, J. M., Lüthgens, C., and Fiebig, M.: Holocene glacier change in the Silvretta Massif (Austrian Alps) constrained by a new 10Be chronology, historical records and modern
525   observations, Quat. Sci. Rev., 245, 106493, 2020.

Braumann, S. M., Schaefer, J. M., Neuhuber, S. M., Lüthgens, C., Hidy, A. J., and Fiebig, M.: Early Holocene cold snaps and their expression in the moraine record of the eastern European Alps, Clim. Past, 17, 2451–2479, 2021.

Braumann, S. M., Schaefer, J. M., Neuhuber, S., and Fiebig, M.: Moraines in the Austrian Alps record repeated phases of glacier stabilization through the Late Glacial and the Early Holocene, Sci. Rep., 12, 9438, 2022.

530   Cecile, M. P. and Abbott, J. G.: Geology of the Niddery Lake map area [NTS 105-O], https://doi.org/10.4095/130689, 1989.

Clarke, G. K. C., Jarosch, A. H., Anslow, F. S., Radić, V., and Menounos, B.: Projected deglaciation of western Canada in the twenty-first century, Nat. Geosci., 8, 372–377, 2015.

Cuffey, K. M. and Paterson, W. S. B.: The Physics of Glaciers, Academic Press, 704 pp., 2010.

535   Dahl, S. O. and Nesje, A.: Paleoclimatic implications based on equilibrium-line altitude depressions of reconstructed Younger Dryas and Holocene cirque glaciers in inner Nordfjord, western Norway, Palaeogeogr. Palaeoclimatol. Palaeoecol., 94, 87–97, 1992.

Demuth, M. N., Wilson, P., and Haggarty, D.: Glaciers of the Ragged Range, Nahanni National Park Reserve, Northwest Territories, Canada, in: Global Land Ice Measurements from Space, edited by: Kargel, J. S., Leonard, G.
540   J., Bishop, M. P., Kääb, A., and Raup, B. H., Springer Berlin Heidelberg, Berlin, Heidelberg, 375–383, 2014.

Ditchburn, R. G. and Whitehead, N. E.: The separation of ^{10}Be from silicates, 1994.

Duk-Rodkin, A., Barendregt, R. W., Tarnocai, C., and Phillips, F. M.: Late Tertiary to late Quaternary record in the Mackenzie Mountains, Northwest Territories, Canada: stratigraphy, paleosols, paleomagnetism, and chlorine - 36, Can. J. Earth Sci., 33, 875–895, 1996.

545   Dyke, A. S.: A lichenometric study of Holocene rock glaciers and neoglacial moraines, Frances Lake map area, southeastern Yukon Territory and Northwest Territories, Geological Survey of Canada, 1-33 pp., 1990.

Ednie, M. and Demuth, M. N.: Mass balance results from the Cordillera Glacier-Climate Observing Network, British Columbia, Northwest Territories, and Alberta, for 2015 and 2016 balance years, Geological Survey of

Canada, 2019.

550   Eis, J., van der Laan, L., Maussion, F., and Marzeion, B.: Reconstruction of past glacier changes with an ice-flow
       glacier model: proof of concept and validation, Front. Earth Sci., 9, 77, 2021.

       https://climate.weather.gc.ca, last access: 1 June 2022.

       Fritz, M., Herzschuh, U., Wetterich, S., Lantuit, H., De Pascale, G. P., Pollard, W. H., and Schirrmeister, L.: Late
       glacial and Holocene sedimentation, vegetation, and climate history from easternmost Beringia (northern Yukon
555   Territory, Canada), Quat. Res., 78, 549–560, 2012.

       Goehring, B. M., Menounos, B., Osborn, G., Hawkins, A., and Ward, B.: Reconciling the apparent absence of a Last
       Glacial Maximum alpine glacial advance, Yukon Territory, Canada, through cosmogenic beryllium-10 and carbon-
       14 measurements, Geochronology, 4, 311–322, 2022.

       Gordey, S. P.: Geology, Little Nahanni River, Northwest Territories-Yukon Territory,
560   https://doi.org/10.4095/184006, 1992.

       Harris, I., Osborn, T. J., Jones, P., and Lister, D.: Version 4 of the CRU TS monthly high-resolution gridded
       multivariate climate dataset, https://doi.org/10.1038/s41597-020-0453-3, 2020.

       Hawkins, A. C., Menounos, B., Goehring, B. M., Osborn, G. D., Clague, J. J., and Jensen, B.: Tandem dating
       methods constrain late Holocene glacier advances, southern Coast Mountains, British Columbia, Quat. Sci. Rev.,
565   274, 107282, 2021.

       Hersbach, H., Bell, B., Berrisford, P., Hirahara, S., Horányi, A., Muñoz-Sabater, J., Nicolas, J., Peubey, C., Radu,
       R., Schepers, D., Simmons, A., Soci, C., Abdalla, S., Abellan, X., Balsamo, G., Bechtold, P., Biavati, G., Bidlot, J.,
       Bonavita, M., Chiara, G., Dahlgren, P., Dee, D., Diamantakis, M., Dragani, R., Flemming, J., Forbes, R., Fuentes,
       M., Geer, A., Haimberger, L., Healy, S., Hogan, R. J., Hólm, E., Janisková, M., Keeley, S., Laloyaux, P., Lopez, P.,
570   Lupu, C., Radnoti, G., Rosnay, P., Rozum, I., Vamborg, F., Villaume, S., and Jean-Noël Thépaut: The ERA5 global
       reanalysis, Quart. J. Roy. Meteor. Soc., 146, 1999–2049, 2020.

       Huang, S., Pollack, H. N., and Shen, P. Y.: Temperature trends over the past five centuries reconstructed from
       borehole temperatures, Nature, 403, 756–758, 2000.

       Hugonnet, R., McNabb, R., Berthier, E., Menounos, B., Nuth, C., Girod, L., Farinotti, D., Huss, M., Dussaillant, I.,
575   Brun, F., and Kääb, A.: Accelerated global glacier mass loss in the early twenty-first century, Nature, 592, 726–731,
       2021.

       Ivy-Ochs, S., Kerschner, H., Maisch, M., Christl, M., Kubik, P. W., and Schlüchter, C.: Latest Pleistocene and
       Holocene glacier variations in the European Alps, Quat. Sci. Rev., 28, 2137–2149, 2009.

       Jarosch, A. H., Schoof, C. G., and Anslow, F. S.: Restoring mass conservation to shallow ice flow models over
580   complex terrain, https://doi.org/10.5194/tc-7-229-2013, 2013.

       Kienholz, C., Rich, J. L., Arendt, A. A., and Hock, R.: A new method for deriving glacier centerlines applied to
       glaciers in Alaska and northwest Canada, Cryosphere, 8, 503–519, 2014.

       Landrum, L., Otto-Bliesner, B. L., Wahl, E. R., Conley, A., Lawrence, P. J., Rosenbloom, N., and Teng, H.: Last
       millennium climate and its variability in CCSM4, J. Clim., 26, 1085–1111, 2013.

585   Luckman, B. H.: The Little Ice Age in the Canadian Rockies, Geomorphology, 32, 357–384, 2000.

       Marcott, S. A., Shakun, J. D., Clark, P. U., and Mix, A. C.: A reconstruction of regional and global temperature for
       the past 11,300 years, Science, 339, 1198–1201, 2013.

       Marzeion, B., Hofer, M., Jarosch, A. H., Kaser, G., and Mölg, T.: A minimal model for reconstructing interannual
       mass balance variability of glaciers in the European Alps, Cryosphere, 6, 71–84, 2012.

590 Maussion, F., Butenko, A., Champollion, N., Dusch, M., Eis, J., Fourteau, K., Gregor, P., Jarosch, A. H., Landmann, J., Oesterle, F., Recinos, B., Rothenpieler, T., Vlug, A., Wild, C. T., and Marzeion, B.: The Open Global Glacier Model (OGGM) v1.1, Geosci. Model Dev., 12, 909–931, 2019.

Meierding, T. C.: Late Pleistocene glacial equilibrium-line altitudes in the Colorado Front Range: a comparison of methods, Quat. Res., 18, 289–310, 1982.

595 Meier, M. F. and Post, A. S.: Recent variations in mass net budgets of glaciers in western North America, International Association of Scientific Hydrology Publications, 58, 63–77, 1962.

Menounos, B., Osborn, G., Clague, J. J., and Luckman, B. H.: Latest Pleistocene and Holocene glacier fluctuations in western Canada, Quat. Sci. Rev., 28, 2049–2074, 2009.

Menounos, B., Goehring, B. M., Osborn, G., Margold, M., Ward, B., Bond, J., Clarke, G. K. C., Clague, J. J.,
600 Lakeman, T., Koch, J., Caffee, M. W., Gosse, J., Stroeven, A. P., Seguinot, J., and Heyman, J.: Cordilleran Ice Sheet mass loss preceded climate reversals near the Pleistocene Termination, Science, 358, 781–784, 2017.

Mood, B. J. and Smith, D. J.: Holocene glacier activity in the British Columbia Coast Mountains, Canada, Quat. Sci. Rev., 128, 14–36, 2015.

Moore, E. M. M., Eaves, S. R., Norton, K. P., Mackintosh, A. N., Anderson, B. M., Dowling, L. H., and Hidy, A. J.:
605 Climate reconstructions for the Last Glacial Maximum from a simple cirque glacier in Fiordland, New Zealand, Quat. Sci. Rev., 275, 107281, 2022.

Moss, R. H., Edmonds, J. A., Hibbard, K. A., Manning, M. R., Rose, S. K., van Vuuren, D. P., Carter, T. R., Emori, S., Kainuma, M., Kram, T., Meehl, G. A., Mitchell, J. F. B., Nakicenovic, N., Riahi, K., Smith, S. J., Stouffer, R. J., Thomson, A. M., Weyant, J. P., and Wilbanks, T. J.: The next generation of scenarios for climate change research
610 and assessment, Nature, 463, 747–756, 2010.

Muñoz-Sabater, J.: ERA5-Land monthly averaged data from 1981 to present, 2019.

Muñoz-Sabater, J.: ERA5-Land monthly averaged data from 1950 to 1980, 2021.

Murray, D. R. and Locke, W. W.: Dynamics of the late Pleistocene Big Timber Glacier, Crazy Mountains, Montana, USA, Journal of Glaciology, 35, 183–190, 1989.

615 Nesje, A.: Topographical effects on the equilibrium-line altitude on glaciers, GeoJournal, 27, https://doi.org/10.1007/bf00185102, 1992.

Nichols, K. A. and Goehring, B. M.: Isolation of quartz for cosmogenic in situ ^{14}C analysis, Geochronology, 1, 43–52, 2019.

Nishiizumi, K., Imamura, M., Caffee, M. W., Southon, J. R., Finkel, R. C., and McAninch, J.: Absolute calibration
620 of ^{10}Be AMS standards, Nucl. Instrum. Methods Phys. Res. B, 258, 403–413, 2007.

Ohmura, A. and Boettcher, M.: Climate on the equilibrium line altitudes of glaciers: theoretical background behind Ahlmann's P/T diagram, J. Glaciol., 64, 489–505, 2018.

Ohmura, A., Kasser, P., and Funk, M.: Climate at the equilibrium line of glaciers, J. Glaciol., 38, 397–411, 1992.

Oien, R. P., Rea, B. R., Spagnolo, M., Barr, I. D., and Bingham, R. G.: Testing the area–altitude balance ratio
625 (AABR) and accumulation–area ratio (AAR) methods of calculating glacier equilibrium-line altitudes, J. Glaciol., 68, 357–368, 2022.

Osmaston, H.: Estimates of glacier equilibrium line altitudes by the Area×Altitude, the Area×Altitude Balance Ratio and the Area×Altitude Balance Index methods and their …, Quat. Int., 138-139, 22–31, 2005.

Pelto, B. M., Menounos, B., and Marshall, S. J.: Multi-year evaluation of airborne geodetic surveys to estimate

630   seasonal mass balance, Columbia and Rocky Mountains, Canada, Cryosph. Discuss., 1–30, 2019.

Pfeffer, W. T., Tad Pfeffer, W., Arendt, A. A., Bliss, A., Bolch, T., Graham Cogley, J., Gardner, A. S., Hagen, J.-O.,
Hock, R., Kaser, G., Kienholz, C., Miles, E. S., Moholdt, G., Mölg, N., Paul, F., Radić, V., Rastner, P., Raup, B. H.,
Rich, J., Sharp, M. J., and The Randolph Consortium: The Randolph Glacier Inventory: a globally complete
inventory of glaciers, https://doi.org/10.3189/2014jog13j176, 2014.

635   Porter, C., Morin, P., Howat, I., Noh, M.-J., Bates, B., Peterman, K., Keesey, S., Schlenk, M., Gardiner, J., Tomko,
K., Willis, M., Kelleher, C., Cloutier, M., Husby, E., Foga, S., Nakamura, H., Platson, M., Wethington, M., Jr,
Williamson, C., Bauer, G., Enos, J., Arnold, G., Kramer, W., Becker, P., Doshi, A., D'Souza, C., Cummens, P.,
Laurier, F., and Bojesen, M.: ArcticDEM, https://doi.org/10.7910/DVN/OHHUKH, 2018.

Porter, S. C.: Equilibrium-line altitudes of late Quaternary glaciers in the Southern Alps, New Zealand,
640   https://doi.org/10.1016/0033-5894(75)90047-2, 1975.

Porter, S. C.: Snowline depression in the tropics during the Last Glaciation, Quat. Sci. Rev., 20, 1067–1091, 2001.

Rounce, D. R., Hock, R., Maussion, F., Hugonnet, R., Kochtitzky, W., Huss, M., Berthier, E., Brinkerhoff, D.,
Compagno, L., Copland, L., Farinotti, D., Menounos, B., and McNabb, R. W.: Global glacier change in the 21st
century: Every increase in temperature matters, Science, 379, 78–83, 2023.

645   Schaefer, J. M., Denton, G. H., Kaplan, M., Putnam, A., Finkel, R. C., Barrell, D. J. A., Andersen, B. G., Schwartz,
R., Mackintosh, A., Chinn, T., and Schlüchter, C.: High-frequency Holocene glacier fluctuations in New Zealand
differ from the northern signature, Science, 324, 622–625, 2009.

Seguinot, J., Rogozhina, I., Stroeven, A. P., Margold, M., and Kleman, J.: Numerical simulations of the Cordilleran
Ice Sheet through the last glacial cycle, Cryosphere, 10, 639–664, 2016.

650   Shea, J. M., Marshall, S. J., and Livingston, J. M.: Glacier distributions and climate in the Canadian Rockies, Arct.
Antarct. Alp. Res., 36, 272–279, 2004.

Sueyoshi, T., Ohgaito, R., Yamamoto, A., Chikamoto, M. O., Hajima, T., Okajima, H., Yoshimori, M., Abe, M.,
O'ishi, R., Saito, F., Watanabe, S., Kawamiya, M., and Abe-Ouchi, A.: Set-up of the PMIP3 paleoclimate
experiments conducted using an Earth system model, MIROC-ESM, Geosci. Model Dev., 6, 819–836, 2013.

655   Taylor, K. E., Stouffer, R. J., and Meehl, G. A.: An overview of CMIP5 and the experiment design, Bull. Am.
Meteorol. Soc., 93, 485–498, 2012.

Tomkins, J. D., Lamoureux, S. F., and Sauchyn, D. J.: Reconstruction of climate and glacial history based on a
comparison of varve and tree-ring records from Mirror Lake, Northwest Territories, Canada, Quat. Sci. Rev., 27,
1426–1441, 2008.

660   Tomkins, M. D., Dortch, J. M., Hughes, P. D., Huck, J. J., Pallàs, R., Rodés, Á., Allard, J. L., Stimson, A. G.,
Bourlès, D., Rinterknecht, V., Jomelli, V., Rodríguez-Rodríguez, L., Copons, R., Barr, I. D., Darvill, C. M., and
Bishop, T.: Moraine crest or slope: An analysis of the effects of boulder position on cosmogenic exposure age, Earth
Planet. Sci. Lett., 570, 117092, 2021.

Yukimoto, S., Kawai, H., Koshiro, T., Oshima, N., Yoshida, K., Urakawa, S., Tsujino, H., Deushi, M., Tanaka, T.,
665   Hosaka, M., Yabu, S., Yoshimura, H., Shindo, E., Mizuta, R., Obata, A., Adachi, Y., and Ishii, M.: The
Meteorological Research Institute Earth System Model Version 2.0, MRI-ESM2.0: Description and basic evaluation
of the physical component, Journal of the Meteorological Society of Japan. Ser. II, 97, 931–965, 2019.

Zemp, M., Nussbaumer, S. U., Gärtner-Roer, I., Bannwart, J., Paul, F., and Hoelzle, M.: Global Glacier Change
Bulletin No. 4 (2018-2019), ISC(WDS)/IUGG(IACS)/UNEP/UNESCO/WMO, World Glacier Monitoring Service,
670   278 pp., https://doi.org/10.5904/wgms-fog-2021-05, 2021.